Calculation of Compressible Adiabatic Turbulent Boundary Layers

TUNCER CEBECI,* A. M. O. SMITH,† AND G. MOSINSKIS‡
Douglas Aircraft Company, Long Beach, Calif.

A method of solution of the compressible turbulent boundary-layer equations for two-dimensional and axisymmetric flows, with transverse-curvature effects, is presented. The Reynolds shear-stress term is eliminated by an eddy-viscosity concept and the time mean of the product of a fluctuating velocity and temperature term appearing in the energy equation is eliminated by an eddy-conductivity concept. An implicit finite-difference method is used in the solution of both momentum and energy equations after they are linearized. Results are presented for several adiabatic compressible flows, with and without pressure gradients for Mach numbers up to 5. The results show that the method is quite accurate and fast; a typical flow can be calculated in one or two minutes on the IBM 360/65 computer.

Nomenclature

c_f = local skin-friction coefficient, $\tau_w/\frac{1}{2}\rho_e u_e^2$
c_p = specific heat at constant pressure
C = viscosity-density parameter, $\rho\mu/\rho_e\mu_e$
f = dimensionless stream function, see Eq. (15)
g = dimensionless total enthalpy ratio, H/H_e
h = specific enthalpy
H = total enthalpy, $h + u^2/2$
k = flow index, = 0 (two-dim. flow) and = 1 (axisym. flow)
k_1,k_2 = constants in eddy-viscosity formulas
K = variable-grid parameter, see Eq. (20)
l = mixing length
L = reference body length
M = Mach number
p = pressure
Pr = Prandtl number, $\mu c_p/\lambda_l$
r = radial distance from axis of revolution
r_0 = body radius
R_x = Reynolds number, $u_e x/\nu_e$
R_θ = Reynolds number, $u_e\theta/\nu_e$
t = transverse-curvature term, $(y\cos\alpha)/r_0$
T = absolute temperature
u = x-component of velocity
v = y-component of velocity
x = distance along body surface measured from leading edge
y = distance normal to x
α = angle between y and r, i.e., slope of body of revolution
β = velocity-gradient parameter, $2\xi/u_e(du_e/d\xi)$
γ = intermittency factor
δ = boundary-layer thickness
δ^* = displacement thickness, $\int_0^\infty \left(1 - \frac{\rho u}{\rho_e u_e}\right) dy$
ϵ = kinematic eddy viscosity
ϵ^+ = ratio of kinematic eddy viscosity to kinematic viscosity, ϵ/ν
η = transformed y-coordinate
θ = momentum thickness, $\int_0^\infty \frac{\rho u}{\rho_e u_e}\left(1 - \frac{u}{u_e}\right) dy$
λ = thermal conductivity
μ = dynamic viscosity
ν = kinematic viscosity
ξ = transformed x-coordinate
ρ = mass density
τ = shear stress
ψ = stream function

Subscripts

c = switching point between the inner and outer eddy-viscosity formulas
i = incompressible
e = outer edge of boundary layer
l = laminar flow
t = turbulent flow
w = wall
∞ = freestream conditions

primes denote differentiation with respect to η

1. Introduction

TO obtain accurate solutions of the boundary-layer equations for laminar and for turbulent flows is quite difficult. For laminar flows the problem is strictly mathematical because the governing differential equations can be written exactly. For this reason highly accurate solutions of the boundary-layer equations are possible. With the advent of high-speed computers, much progress in the calculation of laminar boundary layers has been made, and quite satisfactory results have been obtained.

On the other hand, because of the limited understanding of the turbulent process, the problem of turbulent flow is phenomenological as well as mathematical, and exact solution of the boundary-layer equations is not possible. The boundary-layer equations for such flows contain a term involving the time mean of the product of two fluctuating velocities which is known as the Reynolds shear stress, and a term involving the time mean of the product of a fluctuating velocity and a fluctuating temperature. At the present, these terms have not been rigorously related to the mean velocity and mean temperature distributions. In order to proceed at all, the solutions must depend on some empiricism. Even then the solution of the boundary-layer equations is not easy. Until recently most of the work in this very important area has avoided the mathematical problem and has concentrated on momentum and/or energy integral methods by using various empirical correlations leading to methods with varying degrees of accuracy in predicting boundary-layer parameters.§ The attractive features of these methods are their simplicity and their short computation times. Some of them also can be quite accurate, at least, for two-dimensional incompressible turbulent flows as shown in a special conference on "Prediction Methods for Turbulent Flows" held at Stanford in August 1968. The disadvantages of these methods are that they cannot be readily extended to many important problems such as axisymmetric flows with and without transverse-curvature effects, to flows with heat and mass transfer, to problems with slip at the wall, etc.

Presented as Paper 69-687 at the AIAA Fluid and Plasma Dynamics Conference, San Francisco, Calif., June 16–18, 1969; submitted June 25, 1969; revision received February 24, 1970.

* Senior Engineer/Scientist, Aerodynamics Research. Member AIAA.
† Chief Aerodynamics Engineer for Research, Aerodynamics. Fellow AIAA.
‡ Engineer Scientist, Aerodynamics Research. Associate Fellow AIAA.

§ A summary of these methods as well as other methods that are of differential form is given by Reynolds[1] for two-dimensional incompressible turbulent flows.

The present method eliminates many of the disadvantages of the integral methods by proceeding to solve the full partial-differential equations. While the computation time of the present method is still more than that of an integral method, the difference is quite small and is not a major factor. We use an implicit finite-difference method to solve the boundary-layer equations after we eliminate the Reynolds shear-stress term and the time mean of the fluctuating velocity and temperature by eddy-viscosity and eddy-conductivity concepts, respectively. This formulation has worked quite well for two-dimensional incompressible flows with and without heat transfer as well as axisymmetric flows with transverse-curvature effects, for example, see Refs. 2–5, and hence it is extended to compressible flows. In the formulation, the boundary layer is regarded as a composite layer characterized by inner and outer regions. In the inner region, an eddy viscosity based on Prandtl's mixing length theory is used; in the outer region, a constant eddy viscosity modified by an intermittency factor is used. The eddy-conductivity term is lumped into a "turbulent" Prandtl number that is assumed to be constant and equal to 0.9 in this paper.

In principle, the present method is similar to the ones used by Herring and Mellor[6] and Patankar and Spalding.[7] The main difference between the three methods lies in the eddy-viscosity expression used for each region. In addition, the transformations used to stretch the coordinate normal to the flow direction as well as the numerical method used to solve the boundary-layer equations are considerably different.

It should be pointed out that the present method handles both compressible or incompressible flows with or without heat and mass transfer. The results here are presented only for compressible adiabatic flows. At present the method is being explored for compressible turbulent flows with heat and mass transfer and will be reported later.

2. Basic Equations

2.1 Boundary-Layer Equations

If the normal stress terms are neglected, the compressible turbulent boundary-layer equations for two-dimensional and axisymmetric flows can be written as

continuity

$$\partial/\partial x(r^k\rho u) + \partial/\partial y[r^k(\rho v + \langle\rho' v'\rangle)] = 0 \tag{1}$$

momentum

$$\rho u\frac{\partial u}{\partial x} + (\rho v + \langle\rho' v'\rangle)\frac{\partial u}{\partial y} = \rho_e u_e\frac{du_e}{dx} + \frac{1}{r^k}\frac{\partial}{\partial y}\left[r^k\left(\mu\frac{\partial u}{\partial y} - \rho\langle u'v'\rangle\right)\right] \tag{2}$$

energy

$$\rho u\frac{\partial H}{\partial x} + (\rho v + \langle\rho' v'\rangle)\frac{\partial H}{\partial y} = \frac{1}{r^k}\frac{\partial}{\partial y}\times\left[r^k\frac{\lambda_l}{c_p}\frac{\partial H}{\partial y} - \rho\langle v'H'\rangle + \mu\left(1 - \frac{1}{Pr}\right)u\frac{\partial u}{\partial y}\right] \tag{3}$$

where $k = 0$ for two-dimensional flow and $k = 1$ for axisymmetric flow.

The basic notation and scheme of coordinates are shown in Fig. 1, where u_∞ is a reference velocity, $u_e(x)$ is the velocity just outside the boundary layer, H_e is the total enthalpy outside the boundary layer, and h_e is the local enthalpy outside the boundary layer. The coordinates are a curvilinear system in which x is distance along the surface measured from the stagnation point or leading edge. The dimension y is measured normal to the surface. Within the boundary layer, the velocity components in the x- and y-directions are u and v, respectively. The body radius is r_0.

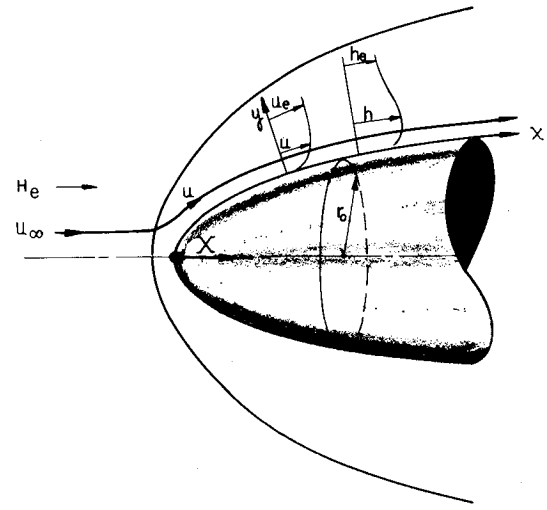

Fig. 1 Coordinate system for the boundary layer on a body of revolution.

In these equations, the transverse-curvature effect (TVC) is retained because of its importance in predicting boundary-layer growth on slender bodies, such as certain missiles or at the tail of a streamlined body of revolution. In such cases the radius of the body may be of the same order of magnitude as the thickness of the boundary layer, and neglect of this effect could be quite important.

The boundary conditions are

momentum

$$u(x,0) = 0,\ v(x,0) = 0, \text{ or } v(x,0) = v_w \text{ (mass transfer)} \tag{4}$$
$$\lim_{y\to\infty} u(x,y) = u_e(x)$$

energy

$$H(x,0) = H_w, \text{ or } \partial H/\partial y(x,0) = (\partial H/\partial y)_w \tag{5}$$
$$\lim_{y\to\infty} H(x,y) = H_e(x)$$

2.2 Formulation of Eddy Viscosity and Turbulent Prandtl Number

In order to solve Eqs. (1–3), it is necessary to relate $-\rho\langle u'v'\rangle$, the Reynolds shear-stress term, and the $-\rho\langle v'H'\rangle$ term to the dependent variables u (or v), and H, respectively. Here we use eddy viscosity (ϵ) and eddy-conductivity (λ_t) concepts, and set $-\rho\langle u'v'\rangle = \rho\epsilon\partial u/\partial y$, $-\rho\langle v'H'\rangle = \rho\lambda_t\,\partial H/\partial y$. The latter expression can also be written as $-\rho\langle v'H'\rangle = \rho\epsilon/Pr_t(\partial H/\partial y)$ by defining the turbulent Prandtl number as $Pr_t = \epsilon/\lambda_t$.

The expression for ϵ in the inner region is based on Prandtl's mixing-length theory; that is,

$$\epsilon_i = l^2|\partial y/\partial y| \tag{6}$$

where l, the mixing length, is given by $l = k_1 y$. A modified expression for l is used in Eq. (6) to account for the viscous sublayer close to the wall. This modification, suggested by Van Driest,[8] is

$$l = k_1 y[1 - \exp(-y/A)] \tag{7}$$

where A is a constant for a given streamwise location in the boundary layer, and is defined as $26\nu(\tau_w/\rho_w)^{-1/2}$, with w denoting values at the wall. Equation (7) was developed for a flat plate. Here we modify the constant A to account for pressure gradient. From the momentum equation it follows that the shear stress close to the wall may be written as

$$\tau = \tau_w + (dp/dx)y \tag{8}$$

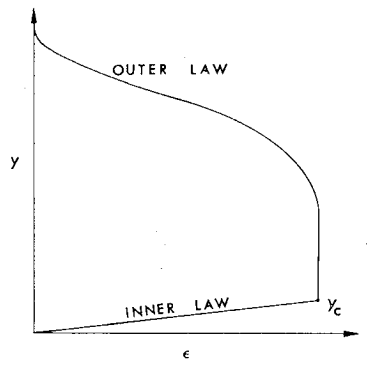

Fig. 2 Eddy-viscosity distribution across a boundary layer.

If A is defined as $26\nu(\tau/\rho)^{-1/2}$, the constant becomes

$$26\nu\left(\frac{\tau_w}{\rho}+\frac{dp}{dx}\frac{y}{\rho}\right)^{-1/2} \tag{9}$$

Then the expression for inner eddy viscosity becomes

$$\epsilon_i = k_1^2 y^2\left\{1-\exp\left[-\frac{y}{26\nu}\left(\frac{\tau_w}{\rho}+\frac{dp}{dx}\frac{y}{\rho}\right)^{1/2}\right]\right\}^2\left|\frac{\partial u}{\partial y}\right| \tag{10}$$

The expression for ϵ in the outer region is based on a constant eddy viscosity, ϵ_0,

$$\epsilon_0 = k_2\int_0^\infty (u_e-u)dy \tag{11}$$

modified by Klebanoff's[8] intermittency factor γ, approximated by the following formula

$$\gamma = \left[1+5.5\left(\frac{y}{\delta}\right)^6\right]^{-1} \tag{12}$$

which is a convenient and sufficiently accurate approximation to the error function.

The choice of constants k_1 and k_2 in the eddy-viscosity formulas depends slightly on the definition of the boundary-layer thickness δ. As in several previous studies, for example, Refs. 2, 3, the values of the constants k_1 and k_2 are taken to be 0.40 and 0.0168, respectively, and δ is defined as the y-distance for which $f' = 0.995$.

The constraint used to define the inner and outer regions is the continuity of the eddy viscosity; from the wall outward, the expression for inner eddy viscosity applies until $\epsilon_i = \epsilon_0$. The dividing point is y_c. Figure 2 shows a typical eddy-viscosity variation across the boundary layer for a flat-plate flow.

2.3 Transformation of Boundary-Layer and Eddy-Viscosity Equations

Equations (1–3), which are expressed in the coordinates of the physical plane, require starting profiles, but these equations are singular at $x = 0$. For this reason, we first transform them as in the previous study,[2] to a coordinate system that removes the singularity at $x = 0$, stretches the coordinate normal to the flow direction, and places the equations in an almost two-dimensional form. We use a combination of the Probstein-Elliot[9] and Levy-Lees[10] transformations.

$$d\xi = \rho_e\mu_e u_e(r_0/L)^{2k}dx,\quad d\eta = [\rho u_e/(2\xi)^{1/2}](r/L)^k dy \tag{13}$$

If a stream function ψ is introduced such that

$$\partial\psi/\partial y = (r/L)^k\rho u,\quad \partial\psi/\partial x = -(r/L)^k(\rho v+\langle\rho' v'\rangle) \tag{14}$$

and if ψ is related to a dimensionless stream function f as

$$\psi(x,y) = (2\xi)^{1/2}f(\xi,\eta) \tag{15}$$

then the momentum Eq. (2), and the energy Eq. (3), become

momentum

$$[(1+t)^{2k}C(1+\epsilon^+)f'']' + ff'' + \beta\left[\frac{\rho_e}{\rho}-(f')^2\right] = 2\xi\left(f'\frac{\partial f'}{\partial\xi}-f''\frac{\partial f}{\partial\xi}\right) \tag{16}$$

energy

$$\left\{(1+t)^{2k}C\left[\left(1+\epsilon^+\frac{Pr}{Pr_t}\right)\frac{g'}{Pr}+\frac{u_e^2}{H_e}\left(1-\frac{1}{Pr}\right)f'f''\right]\right\}' + fg' = 2\xi\left(f'\frac{\partial g}{\partial\xi}-g'\frac{\partial f}{\partial\xi}\right) \tag{17}$$

In Eqs. (16) and (17), t is the transverse-curvature term, β the pressure-gradient term, C is the viscosity-density term, and ϵ^+ is the ratio of eddy viscosity to kinematic viscosity. The dependent variables f' and g in Eqs. (16) and (17) are dimensionless velocity and total-enthalpy ratios, respectively, defined as $f' = u/u_e$ and $g = H/H_e$. It can be seen from Eq. (16) and (17) that setting $k = 0$ reduces the boundary-layer equations to two-dimensional form. For axisymmetric flow with no transverse-curvature effect, $k = 1$ and $t = 0$, which indicates that the ratio of r to r_0 is unity, since $r = r_0 + y\cos\alpha$ and t in the physical plane is defined as $t = (y\cos\alpha)/r_0$. Furthermore, if ϵ^+ is zero, Eqs. (16) and (17) reduce to a classical form of the compressible laminar boundary-layer equations.

The present method is developed so that arbitrary fluid properties may be used. In this study, air is treated as a perfect gas, and the fluid properties μ and ρ are assumed to be functions of specific enthalpy only; the specific heat of air at constant pressure, c_p, is assumed to be constant and equal to 6035 ft^2/sec^2°R. The viscosity μ is obtained from Sutherland's law. The density-enthalpy relation is obtained from the equation of state and from the assumption that static pressure remains constant within the boundary layer. Prandtl number is an input to the computer program.

3. Method of Solution

3.1 Solution of the Momentum Equation

Before we solve Eqs. (16) and (17) by an implicit finite-difference method, we first linearize (16). Introducing a translated stream function φ defined by $\varphi = f - \eta$ and replacing the streamwise derivatives by three-point finite-difference formulas at $\xi = \xi_n$, which permits arbitrary spacing in the ξ-direction, we get

$$[(1+t)^{2k}C(1+\epsilon^+)\varphi'']' + (\varphi+\eta)\varphi'' + \beta[(\rho_e/\rho) - (\varphi')^2 - 2\varphi' - 1] = 2\xi[(\varphi'+1)(A_1\varphi' + A_2\varphi'_{n-1} + A_3\varphi'_{n-2}) - \varphi''(A_1\varphi + A_2\varphi_{n-1} + A_3\varphi_{n-2})] \tag{18}$$

where for simplicity, the subscript n is dropped. At $\xi = \xi_n$, the quantities A_1, A_2, and A_3, which are the usual Lagrange interpolation formulas, are known, and the quantities having the subscripts $n-1$ and $n-2$ are known functions of η from solutions obtained at the two previous stations. Thus, at $\xi = \xi_n$, Eq. (18) is an ordinary differential equation in η. There is no problem of starting the solution, because the terms with streamwise derivatives disappear, since $\xi = 0$. At the next station, ξ_1, the three-point formulas are replaced by two-point formulas; at all stations farther downstream the three-point formulas are used.

To linearize Eq. (18), we assume that certain terms that make the equation nonlinear are known from the previous

iteration; that is,

$$[(1 + t)^{2k}C_0(1 + \epsilon^+)_0\varphi'']' + (\varphi_0 + \eta)\varphi'' + \beta[(\rho_e/\rho)_0 - \varphi_0'\varphi' - 2\varphi' - 1] = 2\xi[(\varphi_0' + 1)(A_1\varphi' + A_2\varphi'_{n-1} + A_3\varphi'_{n-2}) - \varphi_0''(A_1\varphi + A_2\varphi_{n-1} + A_3\varphi_{n-2})] \quad (19)$$

the subscript 0 indicates that the function is obtained from a previous iteration.

The solution of Eq. (19) is obtained by an implicit finite-difference method after the dependent variable φ has been replaced by the perturbation terms $\overline{\Delta\varphi} = \varphi - \varphi_0$, $\overline{\Delta\varphi'} = \varphi' - \varphi_0'$, etc.¶ A finite-difference pattern in the shape of a horizontal T involving three points in the ξ-direction and five points in the η-direction is used. See Fig. 3. The resulting algebraic equations are solved by the Choleski matrix method.

3.2 Solution of the Energy Equation

The method of solution of the energy equation is similar to that of the momentum equation. Again the ξ-derivatives are replaced by finite-difference formulas that are identical to those in the momentum equation. The energy equation is also solved by an implicit finite-difference method. However, this time the five points in the η-direction are replaced by three points because the equation is second order. For details of the solution of both the momentum and the energy equations see Ref. 12.

3.3 Variable-Grid Spacing in the η-Direction

The finite-difference formulas used in both the momentum and the energy equations contain a variable grid in the η-direction, which permits shorter steps close to the wall and longer steps away from the wall. The grid has the property that the ratio of lengths of any two adjacent intervals is a constant; that is, $\Delta\eta_i = K\Delta\eta_{i-1}$. The distance to the ith grid line is given by the following formula:

$$\eta_i = h_1(K^i - 1)/(K - 1) \qquad i = 0,1,2,3,\ldots N \quad (20)$$

where h_1 is the length of the first step and $i = N$ when $\eta_i = \eta_\infty$. Figure 4 accurately represents the η-spacing for $\eta_\infty = 100$, $h_1 = 0.01$ and $K = 1.07$.

3.4 Starting the Solution

The present method handles both incompressible and compressible laminar and turbulent flows. The calculations begin at the leading edge or at the stagnation point, where $\xi = 0$, and proceed downstream. At station $\xi = 0$, the flow is laminar, and it becomes turbulent at any specified station where $\xi > 0$ by allowing ϵ^+ to become nonzero. A calculation can also be started at any ξ-location, provided that initial

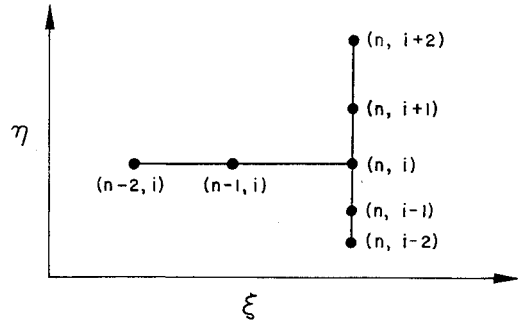

Fig. 3 Finite-difference molecule for the momentum equation at (n,i).

¶ The reason for choosing φ rather than f, and $\Delta\varphi$ rather than φ, is that the round-off errors are reduced.

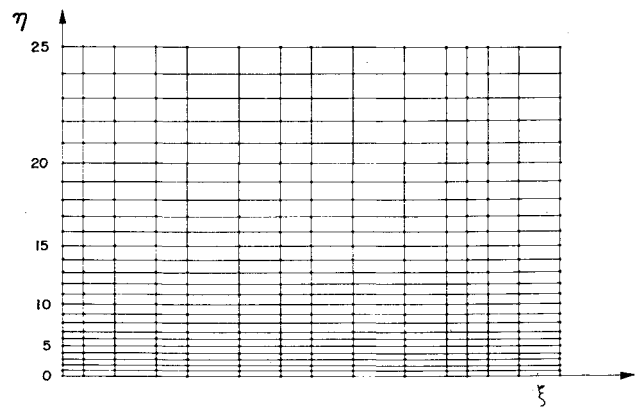

Fig. 4 Finite-difference variable-grid system in the η direction.

velocity and enthalpy profiles are specified. Of course, for incompressible flows with no heat transfer it is only necessary to specify the velocity profile.

Consider the case when initial velocity and enthalpy profiles are known at $\xi = \xi_{n-1}$ and we seek a solution to momentum and energy equations at $\xi = \xi_n$. We first calculate the fluid properties from the enthalpy profiles at $\xi = \xi_{n-1}$ and start the computations from the momentum equation. Before the momentum equation can be solved, it is necessary to establish the inner and outer regions for the eddy-viscosity formulas. Since the eddy-viscosity expressions contain terms like f'' and δ^*, these two regions are not known until a solution of the momentum equation is generated. Thus, an iteration process is necessary. For the first iteration, δ^* and f'' are obtained from the solution at ξ_{n-1}, and inner and outer regions are established by the continuity of the eddy-viscosity equations. With this information, a solution of the momentum equation is obtained and consequently a solution of the energy equation. Then fluid properties are obtained for that particular solution, inner and outer regions for the eddy-viscosity formulas are established and the momentum and energy equations are solved in succession. An iteration procedure based on the convergence of δ^* and f_w'' is used. Figure 5 shows the flow diagrams at $\xi = \xi_n$.

It is important to note that as the calculations proceed downstream, the boundary-layer thickness increases. Since at $\xi = \xi_n$ the initial values of f and its derivatives are obtained from the values at $\xi = \xi_{n-1}$, it is necessary to make an assumption for these values for $\eta > (\eta_\infty)_{n-1}$, where $(\eta_\infty)_{n-1}$ is the transformed boundary-layer thickness at $\xi = \xi_{n-1}$. For this reason, at $\xi = \xi_n$ the values of f and its derivatives are obtained from $\xi = \xi_{n-1}$ up to $\eta = (\eta_\infty)_{n-1}$. For $\eta > (\eta_\infty)_{n-1}$, f is obtained from $f = [\eta - (\eta_\infty)_{n-1} + f_{n-1}(\eta_\infty)]$, f' is assumed

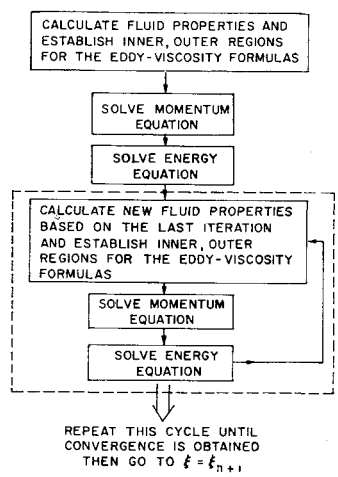

Fig. 5 Flow diagram for solving the boundary-layer equations at $\xi = \xi_n$.

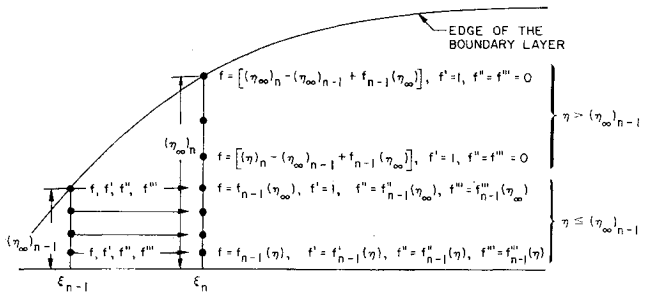

Fig. 6 Diagram showing the method of generating the initial coefficients of the momentum equation at $\xi = \xi_n$.

to be unity, and f'' and f''' are assumed to be zero (see Fig. 6). The latter assumption is accurate, since f'' and f''' approach zero as $\eta \to \eta_\infty$.

4. Accuracy of the Numerical Method

The ultimate test of a numerical method is a comparison of calculated results with exact solutions and with experiments. For laminar flows, there are many analytically obtained solutions, as well as solutions obtained by well-tested and well-established numerical methods. On the other hand, there are no exact solutions for turbulent flows at all, and all one can do is to compare the calculated results with experiments. Since the turbulent boundary-layer equations must contain some empiricism in them because of the fluctuation terms, it is necessary to establish the accuracy of a numerical method before one can investigate the validity of the assumptions made for the fluctuation terms. In addition, it is quite useful to study the characteristics of the numerical method such as computation speed, rate of convergence, etc.

Such a study has been made for the present method in Ref. 12. Various incompressible and compressible laminar flows, and incompressible turbulent flows have been calculated by this method, and comparisons with exact solutions, numerical solutions, as well as experimental flows have been made. In all cases, the method was found to be completely satisfactory for both laminar and turbulent flows. The investigation showed also that the computation time was very small. In general, a typical flow, either laminar or turbulent, consists of about twenty x-stations. The computation time per station is about one second for an incompressible laminar flow and about two to three seconds for an incompressible turbulent flow on the IBM 360/65. Solution of energy equation in either laminar or turbulent flows increases the computation time about one second per station. For further details, such as effect of $\Delta\xi$ and $\Delta\eta$ spacings on the computation time, accuracy, rate of convergence, see Ref. 12.

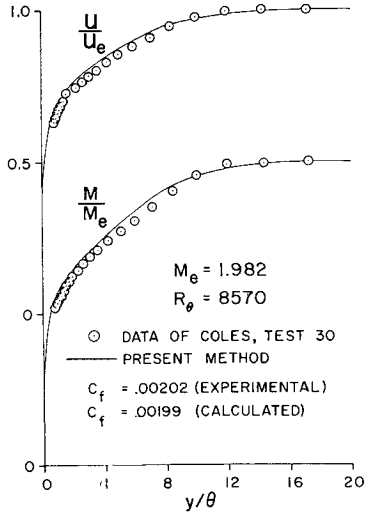

Fig. 7 Comparison of results for the flat-plate flow measured by Coles.[13] Skin friction was measured by floating element.

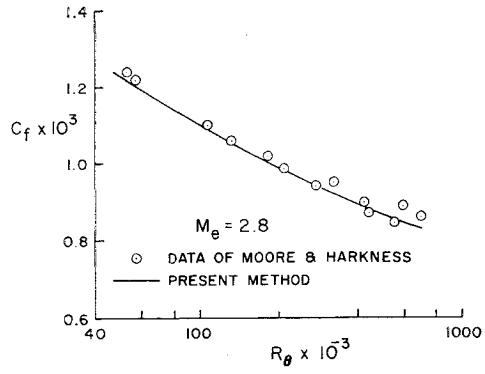

Fig. 8 Comparison of results for the flat-plate flow measured by Moore and Harkness.[14] Skin friction was measured by floating element.

5. Comparison of Calculated and Experimental Results

The method discussed in previous sections has been used to compute a large number of adiabatic compressible turbulent flows. Due to the scarcity of experimental data with pressure gradients, most of the experimental data considered in this paper are flat-plate flows that cover Mach numbers up to 5. Only one two-dimensional accelerating flow and one axisymmetric flow with and without transverse curvature effect is considered.

5.1 Flat-Plate Flows

For constant-velocity flows with different Mach numbers and different momentum-thickness Reynolds numbers, we have considered a large number of experimental data and made comparisons of velocity profiles, Mach profiles, and local skin-friction values. In the latter case, except for a few cases, comparisons were made with those values of local skin-friction coefficient obtained by the floating element technique. Figures 7–15 show comparisons of calculated results with experimental data.

Figure 7 shows a comparison of calculated and experimental velocity and Mach profiles and local skin-friction coefficient for the boundary layer measured by Coles.[13] Skin-

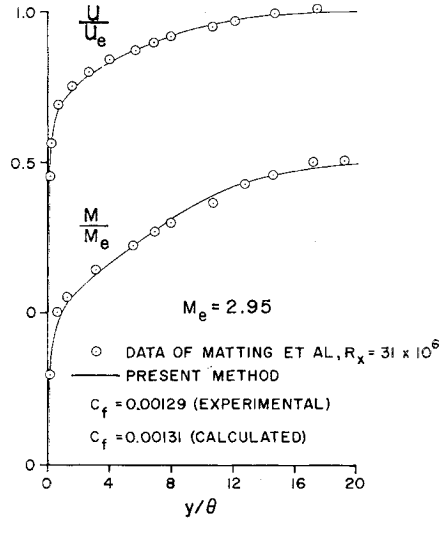

Fig. 9 Comparison of results for the flat-plate flow measured by Matting et al.[15] Skin friction was measured by floating element.

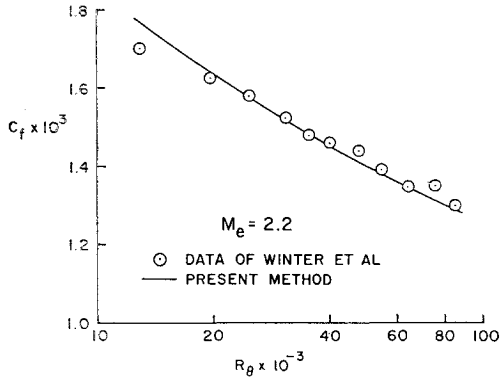

Fig. 10 Comparison of results for the flat-plate flow measured by Winter et al.[16] Skin friction was measured by floating element.

friction coefficients were measured by floating element. Computations in this case and all cases reported in this paper were made by starting the flow to be compressible laminar at $x = 0$, and specifying the flow to be turbulent at the next x-station, which was arbitrarily taken to be $x = 0.001$ ft. The computations were than carried downstream until the experimental R_θ was obtained. Where experimental values of R_θ were not reported, the procedure above was used in matching the experimental R_x. Then at that x-location calculated results were compared with the experimental data.

Figure 8 shows a comparison of local skin-friction values for the boundary layer measured by Moore and Harkness[14] at a nominal $M_e = 2.8$ indicating that agreement is also good for very high Reynolds numbers. The experimental skin-friction was obtained by floating element.

Figure 9 shows a comparison of calculated and experimental velocity and Mach profiles and local-skin-friction coefficient for the boundary layer measured by Matting et al.[15] The experimental skin friction was measured by floating element.

Figure 10 shows a comparison of local skin-friction values for the boundary layer measured by Winter et al[16] at $M_e = 2.2$. The experimental skin-friction values obtained by floating element are in good agreement with the calculated values.

Figure 11 shows a comparison of calculated and experimental velocity and Mach profiles and local-skin-friction value for the boundary layer measured by Stalmach.[17] Again the experimental skin-friction value was obtained by the floating element.

Figure 12 shows a comparison of calculated and experimental velocity and Mach profiles for the boundary layer measured by Nothwang[18] at $M_e = 3.03$.

Figure 13 shows a comparison of calculated and experimental velocity and Mach profiles as well as skin-friction value

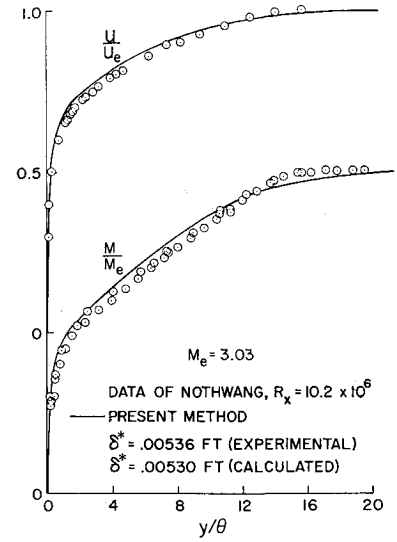

Fig. 12 Comparison of results for the flat-plate flow measured by Nothwang.[18]

for the boundary layer measured by Shutts et al.[19] Experimental profiles as well as experimental skin-friction value obtained by floating element are in good agreement with the calculated results.

Figure 14 shows comparisons of calculated and experimental Mach profiles and momentum-thickness variation for the boundary layer measured by Michel.[20] While the agreement in θ-values is remarkable, the agreement in Mach profiles is only fair.

The present method was also used to calculate the boundary layer measured by Dhawan[21] whose measurements were made at low Mach numbers, 0.2–0.8. Figure 15 shows a comparison of calculated and experimental velocity profiles at three Mach numbers, namely $M_e = 0.41$, 0.635 and 0.795 which correspond to momentum-thickness Reynolds numbers of 1600, 2010, and 2210, respectively, together with a comparison of calculated and experimental skin-friction values, obtained by floating element. The agreement in both cases is good.

5.2 Accelerating Flows

Figure 16 shows the results for an accelerating flow measured by Pasiuk et al.[22] Calculations were started by assuming an adiabatic flat-plate flow that matched the experimental momentum-thickness value at $x = 0.94$ ft. Then the experimental Mach number distribution was used to compute the rest of the flow. The edge Mach number varied from $M_e = 1.69$ at $x = 0.94$ ft to $M_e = 2.97$ at $x = 3.03$ ft. Figure 16a shows a comparison of calculated and experimental displace-

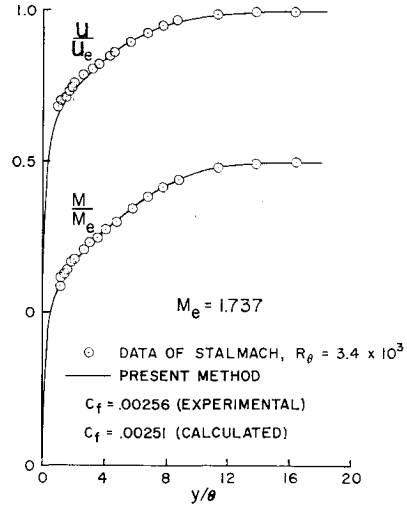

Fig. 11 Comparison of results for the flat-plate flow measured by Stalmach.[17] Skin friction was measured by floating element.

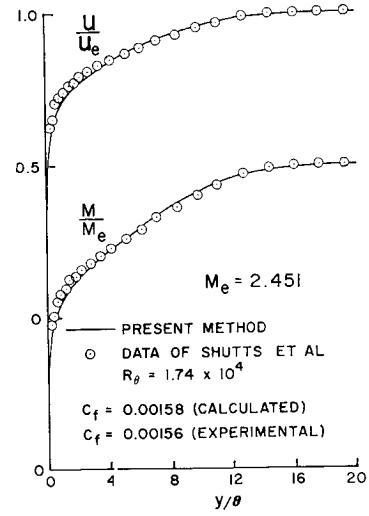

Fig. 13 Comparison of results for the flat-plate flow measured by Shutts et al.[19] Skin friction was measured by floating element.

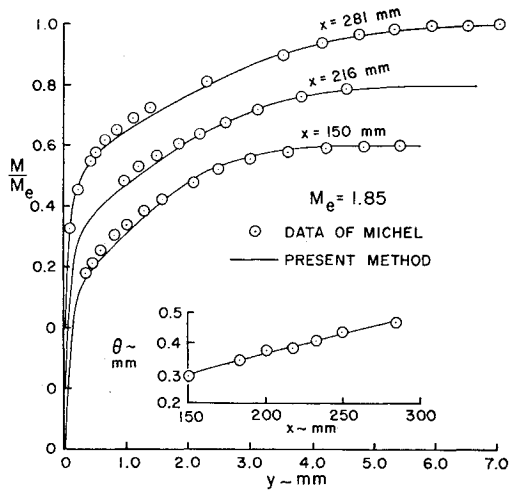

Fig. 14 Comparison of results for the flat-plate flow measured by Michel.[20]

ment thickness and momentum-thickness values together with a comparison of calculated local skin-friction values with those obtained from the momentum integral equation by using the experimental data. Figures 16b and 16c show a comparison of calculated and experimental velocity and temperature profiles, respectively, for three x-stations. While the agreement in velocity profiles and temperature profiles seemed good, the calculated wall temperatures are only in fair agreement with experiment. In dimensionless form they are given in Table 1.

5.3 Axisymmetric Flows with and without Transverse-Curvature Effects

Figure 17 shows the results for a waisted body of revolution measured by Winter, Smith, and Rotta.[23] The experimental skin-friction values were obtained by the "razor blade" technique. The calculations were started by using the experimental velocity profile at $x/L = 0.4$. The enthalpy profile at $x/L = 0.4$ was obtained from the energy equations by using the experimental velocity profile at the same x-location. Calculations were made with and without transverse-curvature effects.

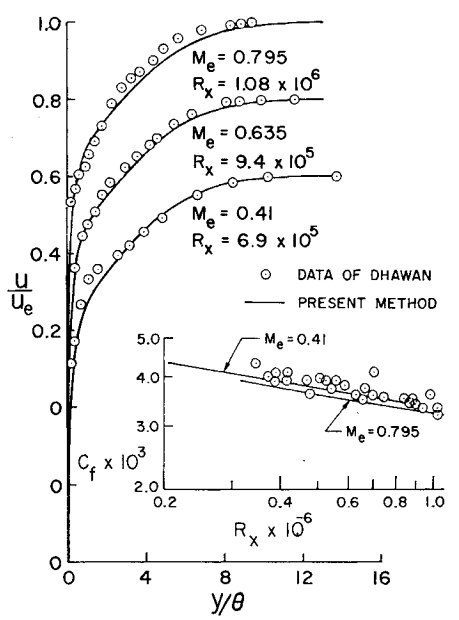

Fig. 15 Comparison of results for the flat-plate flow measured by Dhawan.[21] Skin friction was measured by floating element.

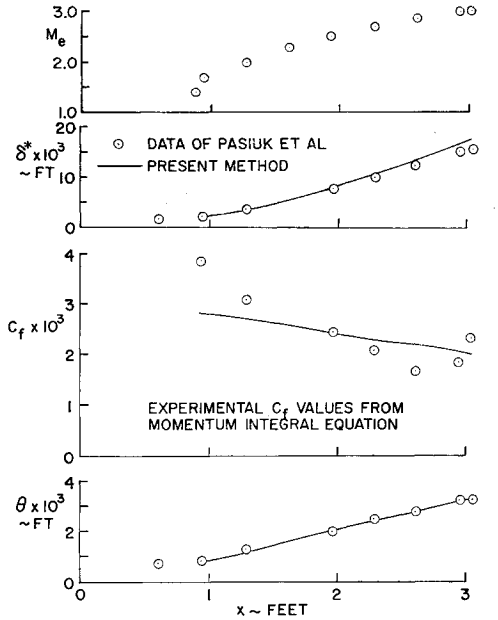

Fig. 16a Comparison of results for the accelerating flow measured by Pasiuk et al.[22]

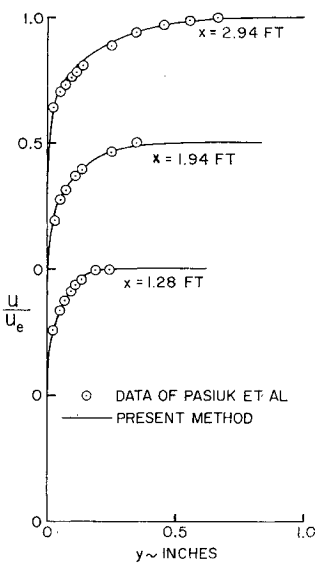

Fig. 16b Comparison of velocity profiles for the flow measured by Pasiuk et al.[22]

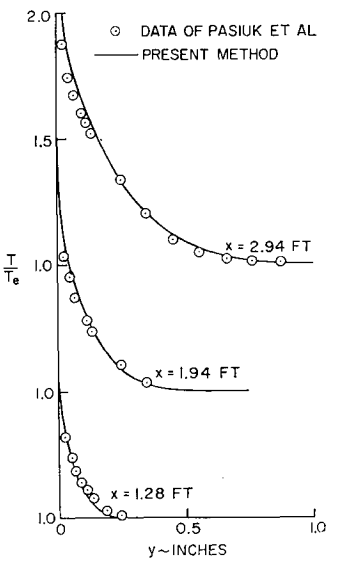

Fig. 16c Comparison of temperature profiles for the flow measured by Pasiuk et al.[22]

Table 1 Comparison of calculated and experimental wall temperatures for the data of Pasiuk et al.[22]

x, ft	$g_{w\text{cal}}$	$g_{w\text{exp}}$	% Error $= \frac{g_{w\text{exp}} - g_{w\text{cal}}}{g_{w\text{exp}}}$
1.94	0.965	0.912	−5.8
2.94	0.958	0.902	−6.2

Figure 17 shows that the calculated skin-friction values are in good agreement with experiment. Whereas the calculated skin-friction values without TVC effect agree quite satisfactorily with the experimental values, the agreement is somewhat better with the TVC effect. The results also show that the effect of transverse curvature markedly affects the momentum-thickness values. Without this TVC effect, the calculated θ-values deviate considerably from the experimental values, especially at locations where the radius of the body is quite small, for example when $x/L = 0.6$–0.8. With the TVC effect, the agreement in θ is much better. It is also interesting to note that the computed θ-values without the TVC effect agree quite well with the calculated θ-values reported in Ref. 23, indicating the importance of transverse-curvature effect.

5.4 Summary of Skin-Friction Results

Figure 18 shows a summary of calculated and experimental skin-friction coefficients for compressible adiabatic turbulent flat-plate flows studied in this paper. The experimental skin-friction values were all measured by the floating element technique except for those obtained by Kistler,[24] which were obtained from velocity profiles. The calculated values cover a Mach number range of 0.41 to 4.67 and a momentum-thickness Reynolds number range of 1.6×10^3 to 702×10^3. The rms error based on 43 experimental values, all obtained by the floating element technique, is 3.5%, which is within the experimental scatter.

Figure 19 shows a comparison of the ratio of calculated and experimental compressible skin-friction coefficient to its incompressible value at the same x-Reynolds number as a function of Mach number together with the Spalding-Chi correlation.[25] The incompressible skin friction values were obtained from Ref. 26. The calculated and experimental skin-friction ratios compare quite well. It is remarkable that when the calculated values deviate from the Spalding-Chi correlation, so do the experimental values.

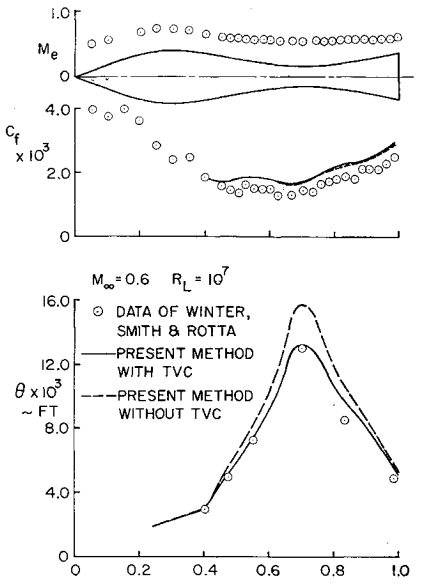

Fig. 17 Comparison of results for the waisted body of revolution measured by Winter, Smith, and Rotta.[23] The skin-friction values were obtained by the "razor blade" technique.

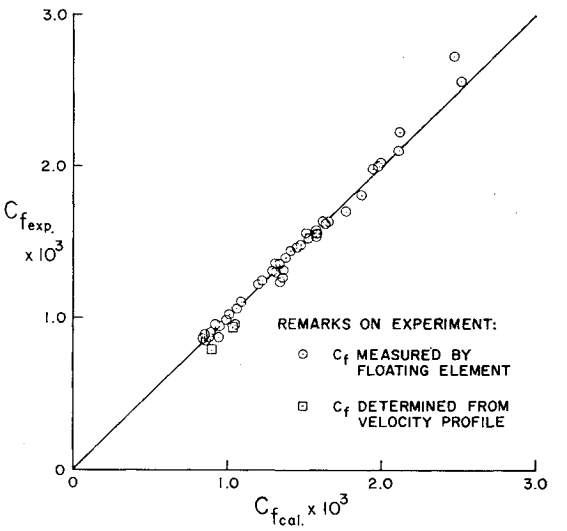

Fig. 18 Comparison of calculated and experimental local skin-friction values. The rms error based on 43 experimental values obtained by the floating element technique is 3.5%.

6. Concluding Remarks

A numerical solution of the turbulent-boundary-layer equations based on a particular eddy-viscosity formulation and the assumption of a constant turbulent Prandtl number is presented for compressible flows with no heat transfer. A large number of flows computed by this method[27] show that the method is quite accurate, as it was in incompressible flows with and without heat transfer. It is remarkable that a simple eddy-viscosity formulation based on flat-plate data can give such satisfactory results.

While it is difficult to say to what low Reynolds numbers the present eddy-viscosity formulation holds true, the results indicate that to R_θ-values as small as 1600 the calculated results agree quite well with experiment.

The results further indicate that the present eddy-viscosity formulation accounts quite well for the effect of compressibility, at least within the Mach number range considered. Figure 20 shows a comparison of two calculated velocity pro-

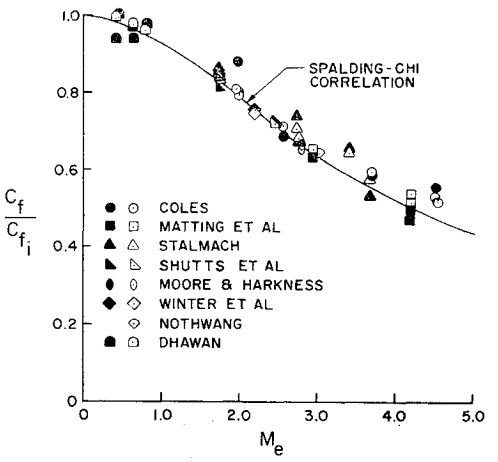

Fig. 19 Comparison of skin-friction variation with Mach number. Open symbols denote the calculated values and the solid symbols denote the experimental values.

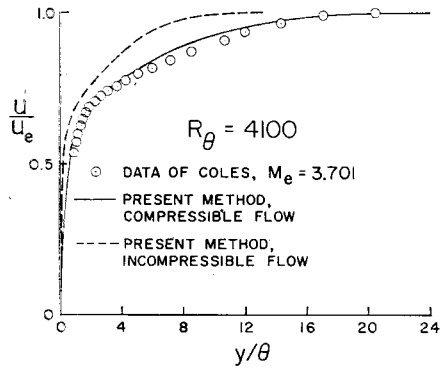

Fig. 20 Compressibility effect on the velocity profiles. Experimental data is due to Coles.[13]

files at the same R_ϑ, one for incompressible and the other for compressible flow. Due to the compressibility effect, the difference between the two profiles is quite appreciable, and eddy-viscosity accounts very well for this effect.

References

[1] Reynolds, W. C., "A Morphology of the Prediction Methods," *Proceedings of the 1968 AFOSR-IFP-Stanford Conference on Computation of Turbulent Boundary Layers*, Vol. 1, Stanford Univ., pp. 1–15.

[2] Smith, A. M. O. and Cebeci, T., "Solution of the Boundary-Layer Equations for Incompressible Turbulent Flow," *Proceedings of the 1968 Heat Transfer and Fluid Mechanics Institute*, 1968, Stanford Univ. Press, pp. 174–191.

[3] Cebeci, T. and Smith, A. M. O., "A Finite-Difference Solution of the Incompressible Turbulent Boundary-Layer Equations by an Eddy-Viscosity Concept," *Proceedings of the 1968 AFOSR-IFP-Stanford Conference on Computation of Turbulent Boundary Layers*, Vol. 1, Stanford Univ., pp. 346–355.

[4] Cebeci, T., Smith, A. M. O., and Mosinskis, G., "Solution of the Incompressible Turbulent Boundary-Layer Equations with Heat Transfer," Paper 69-HT-7, Aug. 1969, ASME; also 5520, March 1969, McDonnell Douglas Corp., Long Beach, Calif.

[5] Cebeci, T., "Laminar and Turbulent Incompressible Boundary Layers on Slender Bodies of Revolution in Axial Flow," Paper 69-WA/FE-2, ASME; also Paper 5524, 1968, McDonnell Douglas Corp., Long Beach, Calif.

[6] Herring, H. J. and Mellor, G. L., "A Method of Calculating Compressible Turbulent Boundary Layers," CR-1144, Sept. 1968, NASA.

[7] Patankar, S. V. and Spalding, D. B., "The Hydrodynamic Turbulent Boundary Layer on a Smooth Wall, Calculated by a Finite-Difference Method," *Proceedings of the 1968 AFOSR-IFP-Stanford Conference on Computation of Turbulent Boundary Layers*, Vol. 1, Stanford Univ., pp. 356–365.

[8] Van Driest, E. R., "On Turbulent Flow Near a Wall," *Journal of the Aeronautical Sciences*, Vol. 23, No. 11, Nov. 1956, pp. 1007–1011.

[9] Klebanoff, P. S., "Characteristics of Turbulence in a Boundary Layer with Zero Pressure Gradient," TN 3178, July 1954, NACA.

[10] Probstein, R. F. and Elliott, D., "The Transverse Curvature Effect in Compressible Axially Symmetric Laminar Boundary-Layer Flow," *Journal of the Aeronautical Sciences*, Vol. 23, 1956, pp. 208–224.

[11] Hayes, W. D. and Probstein, R. F., *Hypersonic Flow Theory*, Academic Press, New York and London, 1959, p. 290.

[12] Cebeci, T. and Smith, A. M. O., "A Finite-Difference Method for Calculating Compressible Laminar and Turbulent Boundary Layers," to be published in *Transactions of ASME;* also DAC 67131, March 1969, McDonnell Douglas Corp., Long Beach, Calif.

[13] Coles, D. E., "Measurements in the Boundary Layer on a Smooth Flat Plate in Supersonic Flow, III. Measurements in a Flat Plate Boundary Layer at the Jet Propulsion Laboratory," 20-71, June 1953, Jet Propulsion Laboratory, Institute of Technology, Pasadena, Calif.

[14] Moore, D. R. and Harkness, J., "Experimental Investigation of the Compressible Turbulent Boundary Layer at Very High Reynolds Numbers," 0-7100/4R-9, April 1964, Ling-Temco-Vought Research Center, Dallas, Texas.

[15] Matting, F. W. et al., "Turbulent Skin Friction at High Mach Numbers and Reynolds Numbers in Air and Helium," TR R-82, 1961, NASA.

[16] Winter, K. G., Smith, K. G., and Gaudet, L., "Measurements of Turbulent Skin Friction at High Reynolds Numbers at Mach Numbers of 0.2 and 2.2," AGARDograph 97, Pt. I, May 1965, pp. 97–124.

[17] Stalmach, C. J., Jr., "Experimental Investigations of the Surface Impact Probe Method of Measuring Local Skin Friction at Supersonic Speeds," DRL-410, CF-2675, Jan. 1958, Univ. of Texas Defense Research Lab., Austin, Texas.

[18] Nothwang, G. J., "An Evaluation of Four Experimental Methods for Measuring Mean Properties of a Supersonic Turbulent Boundary Layer," TN 3721, June 1956, NACA.

[19] Shutts, W. H., Hartwig, W. H., and Weiler, J. R., "Turbulent Boundary Layer and Skin-Friction Measurements on a Smooth, Thermally Insulated Flat Plate at Supersonic Speeds," DRL-364, CM-823, Jan. 1955, Univ. of Texas Defense Research Lab., Austin, Texas.

[20] Michel, R., "Résultants sur la couche limite turbulent aux grandes vitesses," Office National d'Etudes et de Recherches Aeronautiques Mémo Technique 22, 1961, Paris, France.

[21] Dhawan, S., "Direct Measurements of Skin Friction," TN 2567, Jan. 1952, NACA.

[22] Pasiuk, L., Hastings, S. M., and Chatham, R., "Experimental Reynolds Analogy Factor for a Compressible Turbulent Boundary Layer with a Pressure Gradient," Naval Ordnance Rept. NOLTR 64-200, Feb. 1965, White Oak, Md.

[23] Winter, K. G., Smith, K. G., and Rotta, J. C., "Turbulent Boundary Layer Studies on a Waisted Body of Revolution in Subsonic and Supersonic Flow," AGARDograph 97, Pt. I, May 1965, pp. 933–962.

[24] Kistler, A. L., "Fluctuation Measurements in Supersonic Turbulent Boundary Layers," 1052, Aug. 1958, Ballistic Research Labs., Aberdeen Proving Ground, Md.

[25] Spalding, D. B. and Chi, S. W., "The Drag of a Compressible Turbulent Boundary Layer on a Smooth Flat Plate with and without Heat Transfer," *Journal of Fluid Mechanics*, Vol. 18, Pt. I, 1964, pp. 117–143.

[26] Coles, D. E., "Measurements in the Boundary Layer on a Smooth Flat Plate in Supersonic Flow, I. The Problem of the Turbulent Boundary Layer," 20-69, June 1953, Jet Propulsion Lab., Institute of Technology, Pasadena, Calif.

[27] Cebeci, T., Smith, A. M. O., and Mosinskis, G., "Calculation of Compressible Adiabatic Turbulent Boundary Layers," AIAA Paper 69-687, San Francisco, Calif., 1969.